Pergamon

Journal of Structural Geology, Vol. 19, No. 8, pp. 1023 to 1036, 1997

PII: S0191-8141(97)00019-9
0191-8141/97 $17.00 + 0.00

Rotation of fabric elements in convergent shear zones, with examples from the southern Appalachians

JOHN R. PRAY and DONALD T. SECOR, JR

Department of Geological Sciences, University of South Carolina, Columbia, SC 29208, U.S.A.

PAUL E. SACKS

INRS-Georessources, C.P. 7500, Ste-Foy, Quebec, Canada G1V4C7

and

HARMON D. MAHER, JR

Department of Geography and Geology, University of Nebraska at Omaha, Omaha, NB 68182, U.S.A.

Abstract—Plane-strain shear zones between rigid walls which do not rotate but which converge and move laterally relative to each other are here-in referred to as *convergent shear zones*. Analysis of the deformation in convergent shear zones indicates the existence of two flow apophyses, one parallel to the shear zone wall and the other inclined to the wall. Modeling of the development of fabrics in convergent shear zones indicates the occurrence of stable orientations in which S and C' do not rotate and are oppositely inclined to the shear-zone boundary. The stable C' orientation is parallel to the inclined flow apophysis and also is parallel to the approach velocity vector of the opposing walls of the shear zone. If it can be demonstrated from field relationships that the walls of a shear zone were rigid and remained parallel, then the occurrence of a flow apophysis inclined in the direction of shear is diagnostic of convergent shear. S and C' fabrics in the Ridge Road and Gundy Creek shear zones of the southern Appalachian Piedmont are interpreted to indicate a convergent shear regime with an approach velocity vector oriented ~ 10–13° clockwise from the strike of the zones. © 1997 Elsevier Science Ltd.

INTRODUCTION

Many naturally occurring shear zones are interpreted to have formed between rigid blocks which do not rotate but which move laterally with respect to each other (Ramsay and Graham, 1970). If material compatibility is maintained within the shear zone and at its walls, and if the deformation is constant volume, then all displacements are parallel to the walls, and the deformation within homogeneous elements of the zone can be modeled as plane-strain *simple* shear (Ramsay and Graham, 1970). Alternatively, if the deformation is not constant volume, displacements within the zone are inclined to the walls, and the rigid blocks bounding the zone must either move closer together or separate with time. Here we refer to such zones as *convergent* shear or *divergent* shear, depending on whether the shear zone narrows or thickens, respectively, with time.

As noted by Bobyarchick (1986), the directions of the real eigenvectors of a velocity matrix are flow apophyses, i.e. they are material lines which do not rotate. Simple shearing may be represented by:

$$\begin{bmatrix} 0 & \dot{\gamma}_{12} \\ 0 & 0 \end{bmatrix}, \tag{1}$$

where $\dot{\gamma}_{12}$ is the shear strain rate of the zone. Eigenanalysis of eqn. (1) (see Appendix A) indicates a single eigenvector parallel to the overall displacement direction of the zone (Fig. 1a). Convergent or divergent shearing may be represented by:

$$\begin{bmatrix} 0 & \dot{\gamma}_{12} \\ 0 & \dot{\epsilon}_{22} \end{bmatrix}, \tag{2}$$

where $\dot{\epsilon}_{22}$ is the dilatancy rate, which is negative for convergent shearing and positive for divergent shearing. Eigenanalysis of eqn. (2) indicates two eigenvectors, one parallel to the walls of the shear zone and the other inclined to the walls. In the case of convergent shearing, the second eigenvector is inclined toward the shearing direction, whereas, in divergent shearing, the second eigenvector is inclined away from the direction of shearing (Fig. 1b & c). As indicated in Fig. 1, simple shearing, convergent shearing and divergent shearing are each characterized by unique flow patterns. It is possible that these flow patterns are manifested as unique rock fabrics which may be used to deduce the boundary constraints operative during development of the shear zone. In this paper, we investigate the kinematics of simple and convergent shear zones, and compare the predicted fabrics with those observed in field situations.

Theoretical models for heterogeneous *simple* shear zones predict the development of a schistosity (S) which is initially inclined to the shear-zone boundaries but which progressively rotates toward parallelism with the shear-zone boundaries. An elongation lineation (L) develops within S and progressively rotates toward the

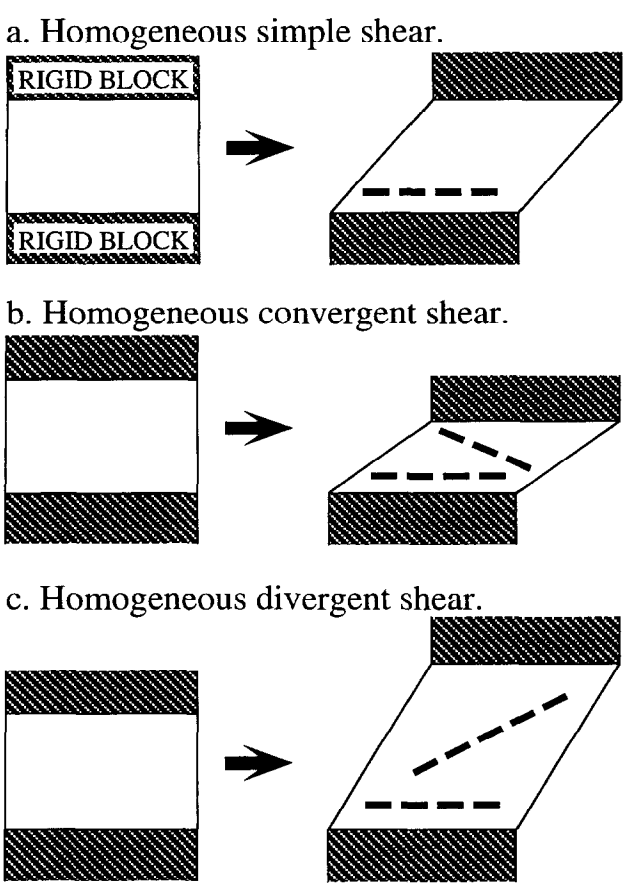

Fig. 1. Illustrations of plane-strain homogeneous simple (a), convergent (b) and divergent (c) shear. The dotted lines illustrate the orientations of flow apophyses.

overall displacement direction for the shear zone (Ramsay and Graham, 1970; Ramsay, 1980). After shear strains of ~ 10, S and L are essentially parallel to the shear-zone boundaries and to the overall displacement direction, within the limits of error of field measurements. These predicted relationships are compatible with field observations in many places (Ramsay and Allison, 1979; Lacassin, 1987; Blenkinsop and Treloar, 1995; Davison *et al.*, 1995). Simple shear zones also often exhibit discrete internal slip surfaces (C-surfaces) oriented parallel to the shear-zone boundary and having the same sense of shear as the zone as a whole (Berthé *et al.*, 1979a; Simpson and Schmid, 1983; Lister and Snoke, 1984).

Some shear zones also contain discrete internal slip surfaces that are inclined in the direction of shear and that have the same sense of shear as the zone as a whole. These are referred to as C'-surfaces (Berthé *et al.*, 1979b; Blenkinsop and Treloar, 1995), shear bands (White *et al.*, 1980), extensional crenulation cleavage (Platt and Vissers, 1980) and normal slip crenulations (Dennis and Secor, 1987). Hereafter, we refer to these inclined slip surfaces as C'.

It is difficult to account for the synkinematic development of a well-defined set of C' surfaces in a high-strain *simple* shear zone because the C' surfaces occupy an unstable orientation that will undergo accelerating rotation away from the shear-zone boundary as deformation progresses (Simpson and De Paor, 1993). However, in convergent shear, there is a flow apophysis inclined in the direction of shear (Fig. 1b). In a convergent shear zone, in which large strains are taking place, C' surfaces that are approximately parallel to the inclined flow apophysis may undergo little or no rotation and may accumulate large shear strains, whereas C' surfaces not parallel to the inclined flow apophyses will rotate away from the apophysis and may be disrupted or inactivated prior to accumulating large shear strain. Under the above circumstances, one expects a preferred orientation of C' planes to develop approximately parallel to the inclined flow apophysis. In this paper, we investigate the possibility that well-developed S-C' fabrics in shear zones are diagnostic of convergent shear boundary conditions.

ANALYTICAL MODEL

In the analysis of heterogeneous deformation within a shear zone, it is usually necessary to partition the shear zone into a set of small elements (Fig. 2), the size of each element being sufficiently small so as to reasonably approximate a homogeneous deformational event (Ramsay and Graham, 1970; Dennis and Secor, 1990, among others). Using this technique a set of linear transformation equations are generated to describe the displacement within an element. The coefficients of these equations may be stored in a matrix for convenience. Displacement matrices may be generated for adjacent elements (maintaining compatibility between elements) within the shear zone in order to account for the heterogeneities. If desired, these individual matrices can be stored as terms (submatrices) in a larger matrix to describe the deformation throughout the shear zone. In the following discussion we will constrain our analysis to a single element which undergoes homogeneous deformation.

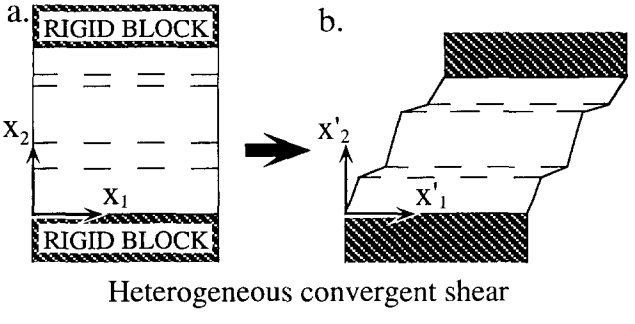

Fig. 2. Diagrams of an idealized dextral, heterogeneous, convergent shear zone, with homogeneous elements parallel to the shear-zone wall. (a) Undeformed block showing the original positions of homogeneous elements. (b) Deformed block. The x_3 co-ordinate axis is perpendicular to the plane of the figure. The deformation is plane strain.

If discrete finite deformational events occur sequentially within a shear zone, the net displacement is path-dependent, and the overall displacement matrix can be composed by combining individual displacement matrices for each event in reverse order of their occurrence using the usual rules for matrix multiplication, viz.:

$$\mathbf{A}_n \ldots \mathbf{A}_3\mathbf{A}_2\mathbf{A}_1 = \prod_{i=n}^{1} \mathbf{A}_i = \mathbf{B}, \tag{3}$$

where $\mathbf{A}_i$ is the displacement matrix for a discrete deformation and $\mathbf{B}$ is the net displacement matrix ($\prod$ is the product operator on a range variable).

However, multiple deformational processes may operate simultaneously within a shear zone (Passchier and Urai, 1988; Wallis, 1992; Fossen and Tikoff, 1993). Furthermore, knowledge of the displacement path often cannot be ascertained. Another useful approach is to examine the velocity field within an element during a period of time in which the velocity components may reasonably be assumed constant. The velocity field equation may then be integrated to obtain analytical solutions for displacement as a function of time. Furthermore, velocity matrices for discrete processes may be summed to obtain an overall velocity matrix, viz.:

$$\mathbf{A}_1 + \mathbf{A}_2 + \mathbf{A}_3 + \ldots \mathbf{A}_n = \sum_{i=1}^{n} \mathbf{A}_i = \mathbf{B}. \tag{4}$$

This allows for the analysis of both discrete processes and the overall deformation. If desired, derived displacement matrices for deformation during sequential periods may be combined following eqn. (3).

Thus far we have described a methodology for modeling the deformation of a heterogeneous shear zone by dividing the shear zone into homogeneous elements, then analyzing the discrete deformational events which operate sequentially in each element, and finally decomposing each of these events into velocity matrices (which may be integrated to obtain displacement fields as functions of time) for different processes which operate simultaneously and which account for all of the effects of the overall deformation. Presently we review the mathematics of a displacement matrix operating on a line or plane, and in the next section develop a model to account for stable S and C' oblique to the walls of a convergent shear zone. A discussion of the use of eigenanalysis for obtaining displacement fields from velocity fields, for determination of irrotational material lines, and for obtaining magnitudes and directions of the finite principal quadratic elongations as functions of time is given in Appendix A.

Let $\mathbf{x}$ be a column vector that has the direction cosines of an arbitrary lineation or unit normal to a plane as its components, and let $\mathbf{L}$ be an arbitrary displacement matrix which accounts for all of the mechanisms which affect the orientation of the line or plane. The direction numbers ($\mathbf{x}'$) following $\mathbf{L}$ are

$$\mathbf{x}' = \mathbf{L}\mathbf{x}, \tag{5}$$

for a lineation and

$$\mathbf{x}' = (\mathbf{x}^{\mathrm{T}}\mathbf{L}^{-1})^{\mathrm{T}}, \tag{6}$$

for a plane (Flinn, 1978). The superscript T represents the transpose of a matrix or vector, primes are vectors after a matrix operation.

The angle (ω) in a co-ordinate plane that the projection of vector $\mathbf{x}$ (or $\mathbf{x}'$) makes with one of the co-ordinate axes may be calculated by:

$$\tan\omega = \tan(x_j, x_i) = \frac{x_j}{x_i}, \tag{7}$$

where x_i is the component of the vector along the co-ordinate axis of interest, and x_j is the other component of the vector in the co-ordinate plane of interest. In the next section we develop a model for deformation within the x_1–x_2 plane of a right-handed co-ordinate system (unless otherwise stated, all angles given are positive when directed counterclockwise from the positive x_1 axis to the vector of interest). Thus, eqn. (7) becomes the familiar:

$$\tan\omega = \frac{x_2}{x_1}. \tag{8}$$

Plane-strain model

In our model we assume a dextral convergent shear zone (Fig. 2). The walls of the shear zone are assumed parallel to the x_1–x_3 co-ordinate axes. All displacements take place in the x_1–x_2 co-ordinate plane. Simple shearing ($\dot{\gamma}_{12}$) is allowed parallel to x_1 and coaxial flattening ($\dot{\epsilon}_{22}$) parallel to x_2. The walls of the shear zone are not permitted to rotate relative to each other ($\dot{\gamma}_{21} = 0$), and stretching of the shear zone walls parallel to x_1 (e.g. Passchier, 1991) is not allowed ($\dot{\epsilon}_{11} = 0$). The net velocity field equation for the shear zone is then given by:

$$\dot{\mathbf{x}} = \dot{\mathbf{D}}\mathbf{x} = \begin{bmatrix} \dot{x}_1 \\ \dot{x}_2 \end{bmatrix} = \begin{bmatrix} 0 & \dot{\gamma}_{12} \\ 0 & \dot{\epsilon}_{22} \end{bmatrix} \begin{bmatrix} x_1 \\ x_2 \end{bmatrix}. \tag{9}$$

The dilational strain rate ($\dot{\Delta}$) within the reference plane for the overall deformation is:

$$\dot{\Delta} = \dot{\epsilon}_{22}. \tag{10}$$

When, as in this case, $\dot{\Delta} \neq 0$, a volume change mechanism must be operative in the shear zone. The removal of dissolved material from the shear zone by circulating fluids, for example in the manner envisioned by O'Hara (1988, 1990), is compatible with our plane strain analysis of the solid material in the shear zone.

We allow non-penetrative simple shearing ($\dot{\gamma}_a$), representing slip along C' planes, and oriented at an oblique angle to the shear-zone boundaries. C' will occur in parallel sets and be represented by $\mathbf{a}$, where $\mathbf{a}$ is the unit

normal vector to the C' surfaces. The velocity matrix for C' slip will be represented by $\dot{\mathbf{A}}$ where:

$$\dot{\mathbf{A}} = \begin{bmatrix} a_1 a_2 \dot{\gamma}_a & a_2^2 \dot{\gamma}_a \\ -a_1^2 \dot{\gamma}_a & -a_1 a_2 \dot{\gamma}_a \end{bmatrix} \tag{11}$$

(Dennis and Secor, 1990). Because slip on C' is not penetrative, $\dot{\mathbf{A}}$ will not operate on other elements within the shear zone.

Maintenance of boundary conditions requires an additional velocity matrix, $\dot{\mathbf{B}}$ which accounts for all other penetrative processes and satisfies:

$$\dot{\mathbf{x}} = \left(\dot{\mathbf{A}} + \dot{\mathbf{B}}\right)\mathbf{x} = \dot{\mathbf{A}}\mathbf{x} + \dot{\mathbf{B}}\mathbf{x} = \dot{\mathbf{D}}\mathbf{x}; \tag{12}$$

therefore

$$\dot{\mathbf{A}} + \dot{\mathbf{B}} = \dot{\mathbf{D}} \tag{13}$$

and

$$\dot{\mathbf{B}} = \dot{\mathbf{D}} - \dot{\mathbf{A}} = \begin{bmatrix} -a_1 a_2 \dot{\gamma}_a & \dot{\gamma}_{12} - a_2^2 \dot{\gamma}_a \\ a_1^2 \dot{\gamma}_a & \dot{\epsilon}_{22} + a_1 a_2 \dot{\gamma}_a \end{bmatrix}. \tag{14}$$

A velocity field equation may now be written for material in the shear zone that is not operated on by C' slip:

$$\dot{\mathbf{x}} = \dot{\mathbf{B}}\mathbf{x} = \begin{bmatrix} \dot{x}_1 \\ \dot{x}_2 \end{bmatrix} = \begin{bmatrix} -a_1 a_2 \dot{\gamma}_a & \dot{\gamma}_{12} - a_2^2 \dot{\gamma}_a \\ a_1^2 \dot{\gamma}_a & \dot{\epsilon}_{22} + a_1 a_2 \dot{\gamma}_a \end{bmatrix} \begin{bmatrix} x_1 \\ x_2 \end{bmatrix}. \tag{15}$$

We now have two velocity field equations: eqn. (9) describes the overall macroscopic behavior of the shear zone and its boundaries, and eqn. (15) describes the mesoscopic behavior of material between C' surfaces that is not operated upon by C' slip. If we assume constant velocities, the differential equations may be solved for the displacement field by the method of eigenanalysis (see Appendix A). This method also gives additional information on material behavior. As noted by Bobyarchick (1986), the real eigenvectors of the velocity matrix are the flow apophyses: i.e. material lines parallel to the real eigenvectors do not rotate. From this, we may deduce that, in plane strain, planes parallel to both the x_3 coordinate axis and a real eigenvector will not rotate.

The eigenvectors (vs) and corresponding eigenvalues (λs) of $\dot{\mathbf{D}}$ are:

$$\begin{aligned} \mathbf{v}_1 &= \begin{bmatrix} 1 \\ 0 \end{bmatrix} \text{ for } \lambda_1 = 0 \\ \mathbf{v}_2 &= \begin{bmatrix} \dot{\gamma}_{12} \\ \dot{\epsilon}_{22} \end{bmatrix} \text{ for } \lambda_2 = \dot{\epsilon}_{22}. \end{aligned} \tag{16}$$

The first eigenvector for $\dot{\mathbf{D}}$ is parallel to the shear-zone boundaries. The second eigenvector will be inclined to the shear-zone boundaries when $\dot{\epsilon}_{22} \neq 0$. Furthermore, the normal to a plane which contains the inclined eigenvector and is parallel to the x_3 axis will be inclined at a counterclockwise angle α_{ss} to the x_1 axis where:

$$\tan \alpha_{ss} = \frac{\dot{\gamma}_{12}}{-\dot{\epsilon}_{22}}. \tag{17}$$

From eqn. (A20), the solution of eqn. (9) for $\mathbf{x}(t)$ may be written:

$$\begin{aligned} \mathbf{x}(t) = \mathbf{D}\mathbf{x}(0) &= \begin{bmatrix} x_1(t) \\ x_2(t) \end{bmatrix} \\ &= \begin{bmatrix} 1 & \tan \alpha_{ss}\left(1 - e^{\dot{\epsilon}_{22} t}\right) \\ 0 & e^{\dot{\epsilon}_{22} t} \end{bmatrix} \begin{bmatrix} x_1(0) \\ x_2(0) \end{bmatrix}. \end{aligned} \tag{18}$$

The terms on the principal diagonal of $\mathbf{D}$ are the finite stretches parallel to the respective co-ordinate axes, whereas the upper right-hand term is the finite shear strain parallel to the shear-zone boundaries. The assumption of constant velocity requires that a_1 and a_2 in eqn. (15) do not vary. This occurs when C' is parallel to either eigenvector of $\dot{\mathbf{D}}$. When C' is in the inclined steady-state position (α_{ss}) then:

$$a_1 = \cos \alpha_{ss} = \frac{\dot{\epsilon}_{22}}{\sqrt{\dot{\epsilon}_{22}^2 + \dot{\gamma}_{12}^2}} \tag{19a}$$

$$a_2 = \sin \alpha_{ss} = \frac{-\dot{\gamma}_{12}}{\sqrt{\dot{\epsilon}_{22}^2 + \dot{\gamma}_{12}^2}}. \tag{19b}$$

By substitution of the above constraints into eqn. (15), and use of the Pythagorean identity for direction cosines, the eigenvectors and corresponding eigenvalues for $\dot{\mathbf{B}}$ may be expressed as:

$$\begin{aligned} \mathbf{v}_1 &= \begin{bmatrix} -\tan \alpha_{ss} \\ 1 \end{bmatrix} \text{ for } \lambda_1 = \dot{\epsilon}_{22} \\ \mathbf{v}_2 &= \begin{bmatrix} -\tan \beta_{ss} \\ 1 \end{bmatrix} \text{ for } \lambda_2 = 0, \end{aligned} \tag{20}$$

where

$$\tan \beta_{ss} = \frac{\dot{\epsilon}_{22}^2 - \dot{\gamma}_a \dot{\gamma}_{12} + \dot{\gamma}_{12}^2}{\dot{\gamma}_a \dot{\epsilon}_{22}}. \tag{21}$$

Thus a plane in the material between C' surfaces will not rotate when the normal to the foliation is oriented at a counterclockwise angle to the positive x_1 axis of either α_{ss} or β_{ss}. The solution of eqn. (15) for position as a function of time, $\mathbf{x}(t)$, may therefore be written as:

$$\begin{aligned} \begin{bmatrix} x_1(t) \\ x_2(t) \end{bmatrix} &= \frac{1}{\tan \beta_{ss} - \tan \alpha_{ss}} \\ &\times \begin{bmatrix} \tan \beta_{ss} - \tan \alpha_{ss} e^{\dot{\epsilon}_{22} t} & \tan \alpha_{ss} \tan \beta_{ss}\left(1 - e^{\dot{\epsilon}_{22} t}\right) \\ e^{\dot{\epsilon}_{22} t} - 1 & \tan \beta_{ss} e^{\dot{\epsilon}_{22} t} - \tan \alpha_{ss} \end{bmatrix} \\ &\times \begin{bmatrix} x_1(0) \\ x_2(0) \end{bmatrix}. \end{aligned} \tag{22}$$

In addition to the positions of stability for C' and foliation, we may also determine the orientations of these planes at any point in time using eqns (18) and (22), respectively (see Appendix A). The counterclockwise

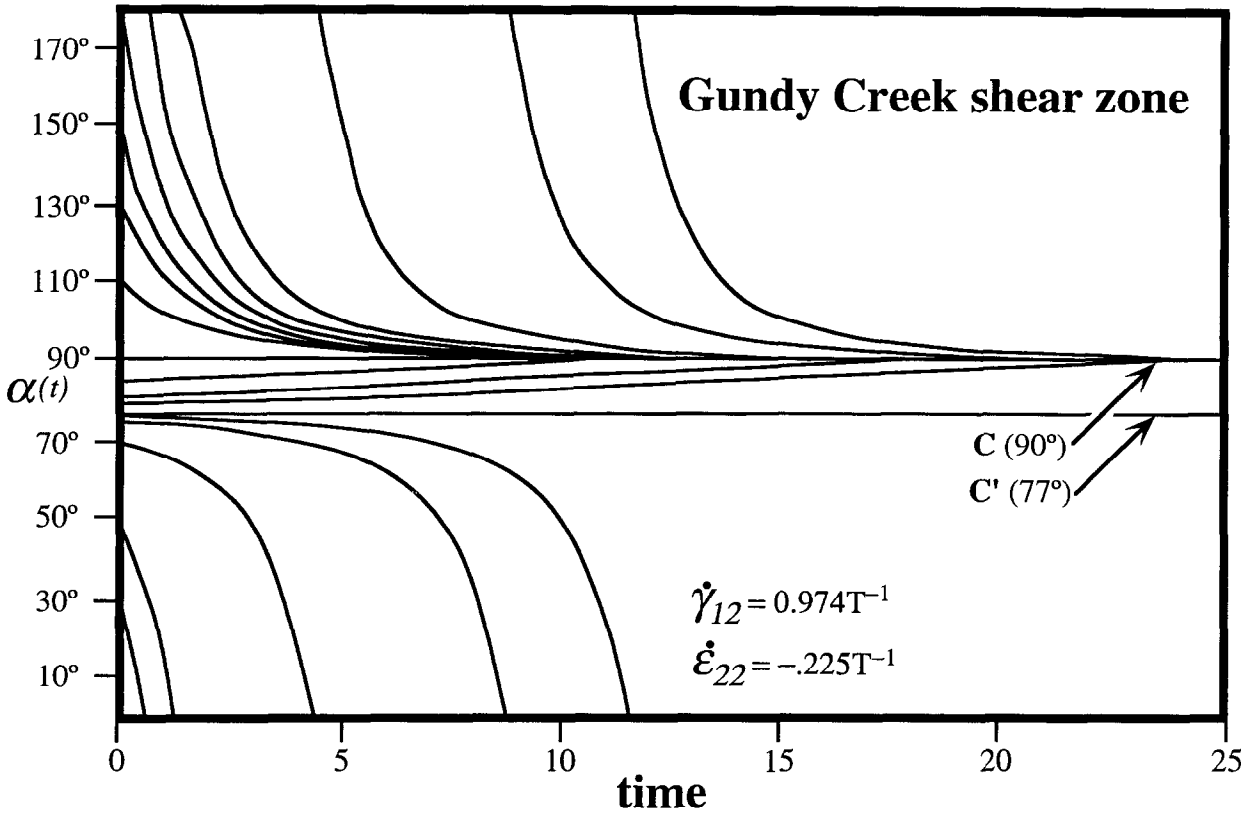

Fig. 3. Illustration of the rotation of C' as a function of time in a convergent shear zone, for various initial C' orientations (α), assuming $\dot{\gamma}_{12} = 0.974T^{-1}$ and $\dot{\epsilon}_{22} = -0.225T^{-1}$. These values are chosen to simulate a preferred C'_4 orientation similar to that observed in the Gundy Creek shear zone. Time units are arbitrary.

angle the normal to C' will make (α_t) at any point in time with the shear-zone boundaries is given by:

$$\tan \alpha_t = \frac{\tan \alpha_0 - \tan \alpha_{ss}}{e^{\dot{\epsilon}_{22} t}} + \tan \alpha_{ss}, \qquad (23)$$

where α_0 is the initial orientation of the normal to C'. An example of the rotation of C' with time is illustrated in Fig. 3. Similarly, assuming C' is in its stable position, the angle (β_t) that a material plane will make with the positive x_1 axis with time is:

$$\tan \beta_t \frac{\tan \beta_{ss}(\tan \beta_0 - \tan \alpha_{ss}) + \tan \alpha_{ss}(\tan \beta_{ss} - \tan \beta_0)e^{\dot{\epsilon}_{22} t}}{(\tan \beta_0 - \tan \alpha_{ss}) + (\tan \beta_{ss} - \tan \beta_0)e^{\dot{\epsilon}_{22} t}}, \qquad (24)$$

given the initial angle β_0. An example of the rotation of material planes for various initial orientations is shown in Fig. 4. The orientation of the normal to the flattening plane of material bounded by C' and the shear-zone boundaries is also shown in Fig. 4, demonstrating that with time, material planes will rotate into an orientation parallel to the flattening plane.

APPLICATION TO FIELD SITUATIONS

Application of the above model to field situations is critically dependent on the validity of the assumptions made in the model. If it can be demonstrated that the bounding blocks of the shear zone were rigid and did not rotate relative to each other during the course of the deformation, and if material compatibility was maintained within the shear zone and at its walls, then the deformation within homogeneous elements of the shear zone would be either plane-strain *simple* shear, *convergent* shear or *divergent* shear. If a flow apophysis inclined in the direction of shear is inferred from the presence of a well-defined set of C' surfaces, then the deformation would have to be convergent shear (Fig. 1) with the approach velocity of the opposing walls of the shear parallel to the inclined apophysis.

For convergent shear, the model predicts two flow apophyses, one parallel to the walls and one parallel to the approach velocity vector of the opposing walls of the shear zone. C or C' planes that form approximately parallel to flow apophyses may accumulate finite strain with little or no rotation. C' planes that form in the acute angle between the flow apophyses (Fig. 5) will slowly rotate into near parallelism with the wall while accumulating finite strain. C' planes that are more steeply inclined to the wall than the inclined flow apophysis will undergo accelerating rotation away from the apophysis, and may cease slipping or may be disrupted before accumulating finite strain.

The above model predicts steady-state fabric relationships that are similar to ones commonly observed in the field. In a convergent shear zone, there are two different

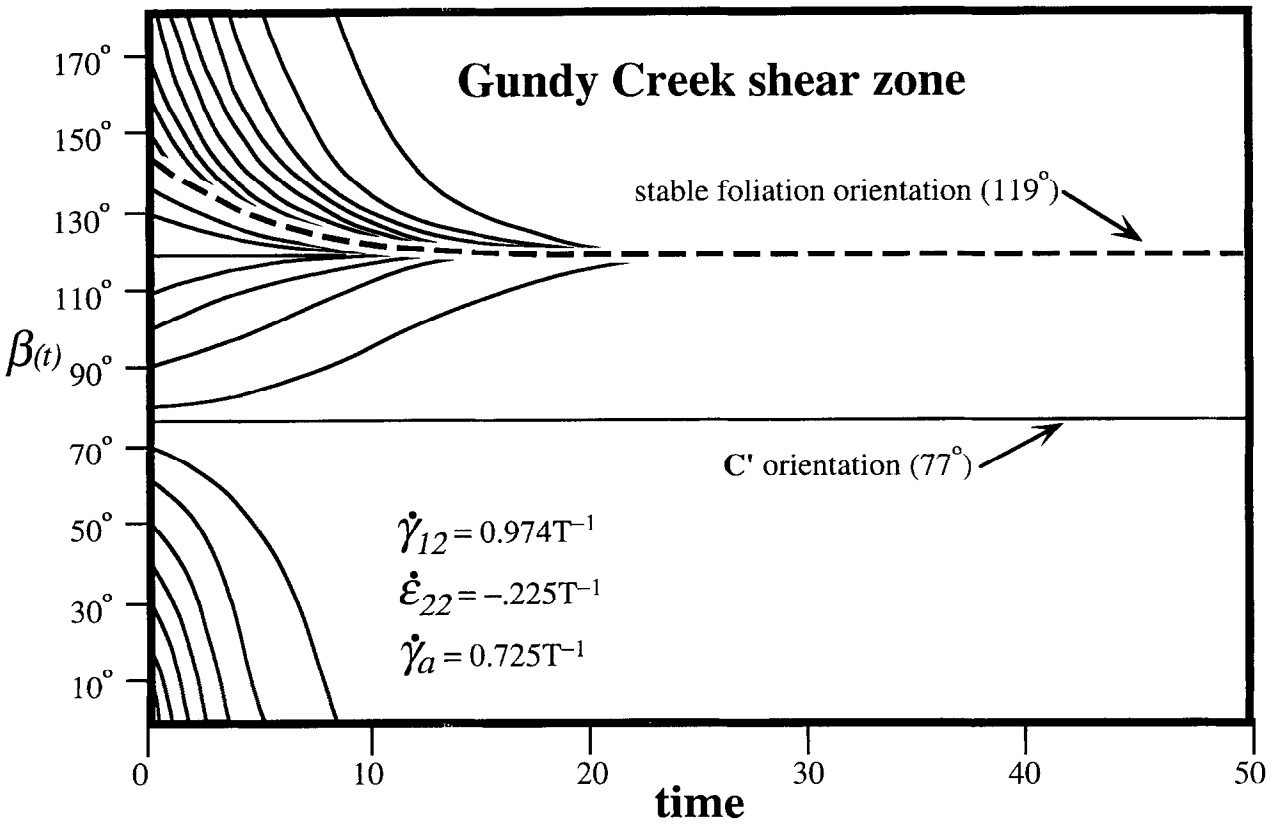

Fig. 4. Illustration of the rotation of the flattening plane (dotted line), and material planes (β_t) for various initial orientations, as functions of time in a convergent shear zone. Note that as the shear zone approaches the steady-state configuration, the material planes will rotate into parallelism with the flattening plane. Assumed strain rates ($\dot{\gamma}_{12} = 0.974T^{-1}$, $\dot{\varepsilon}_{22} = -0.225T^{-1}$ and $\dot{\gamma}_a = 0.725T^{-1}$) were chosen to simulate a preferred foliation orientation similar to that observed in the Gundy Creek shear zone. Time units are arbitrary.

steady-state fabric configurations that may develop (Fig. 5). In the first configuration, C and S are both nearly parallel to the shear-zone boundary. In the second configuration, C' and S are oppositely inclined to the shear-zone boundary, and C' is oriented parallel to the relative velocity vector of the opposing walls of the shear zone. The first configuration may develop either in simple shear or in convergent shear. The second configuration is diagnostic of convergent shear. In theory, the steady-state configurations illustrated in Fig. 5 are developed only after an infinite amount of deformation has taken place. However, we suggest that fabrics diagnostic of convergent shear can be recognized after only moderate shear strain. The sufficient criteria for convergent shear between rigid non-rotating walls are a strong preferred orientation of C' inclined in the shear direction, together with a strong preferred orientation of S inclined to the shear-zone boundary in a sense opposite to that of C'.

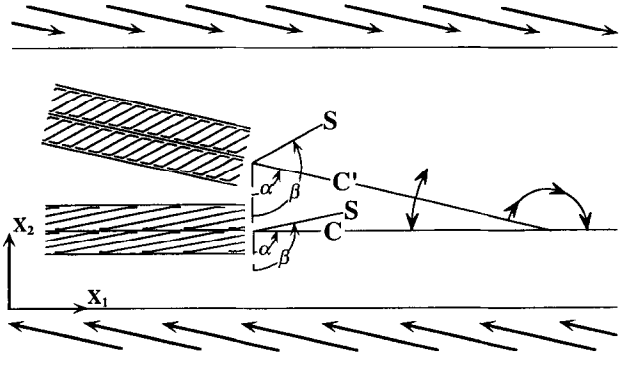

Fig. 5. Sketch showing the two possible stable configurations for C or C' in a dextral convergent shear zone. The inclined C' surfaces are parallel to the relative velocity vector of the opposing walls of the shear zone. C' surfaces that form in other orientations will rotate in the directions shown by the arrows.

Analyses of displacement matrices that are more general than those assumed for convergent shear (i.e. matrices in which stretching and/or rotation of the walls are permitted) indicate that inclined flow apophyses may occur under these more general conditions. It is possible that an inclined flow apophysis in a *general* shear zone might also be recognized from a strong preferred orientation of C' planes. However, in a general shear zone, an inclined flow apophysis is not necessarily parallel to the relative approach velocity vector of the walls. In order to infer the approach velocity vector of the walls of a shear zone, it is necessary to show that the bounding blocks of the shear zone were rigid and did not

rotate relative to each other during the development of the zone.

EXAMPLES IN THE EASTERN APPALACHIAN PIEDMONT

Ductile shear zones with *C′* surfaces are exceptionally well developed along the boundary between the Carolina and Savannah River terranes in the eastern Appalachian Piedmont (Secor and Snoke, 1978; Secor *et al.*, 1986; Dennis and Secor, 1987; Dennis *et al.*, 1987). Here we describe two examples (the Ridge Road and Gundy Creek shear zones) that are well exposed along the shores of J. Strom Thurmond Lake on the Savannah River (Fig. 6).

The Carolina and Savannah River terranes are juxtaposed by the Modoc fault (Maher and Sacks, 1987; Sacks and Dennis, 1987), a regionally extensive ductile shear zone that extends northeastward for 300 km through Georgia and South Carolina. Field and geochronological data (Dallmeyer *et al.*, 1986; Maher and Sacks, 1987; Pray, 1993) are interpreted to indicate that the Modoc shear zone is late Paleozoic, whereas, in the Carolina and Savannah river terranes outside the Modoc shear zone, the last significant ductile deformation occurred before

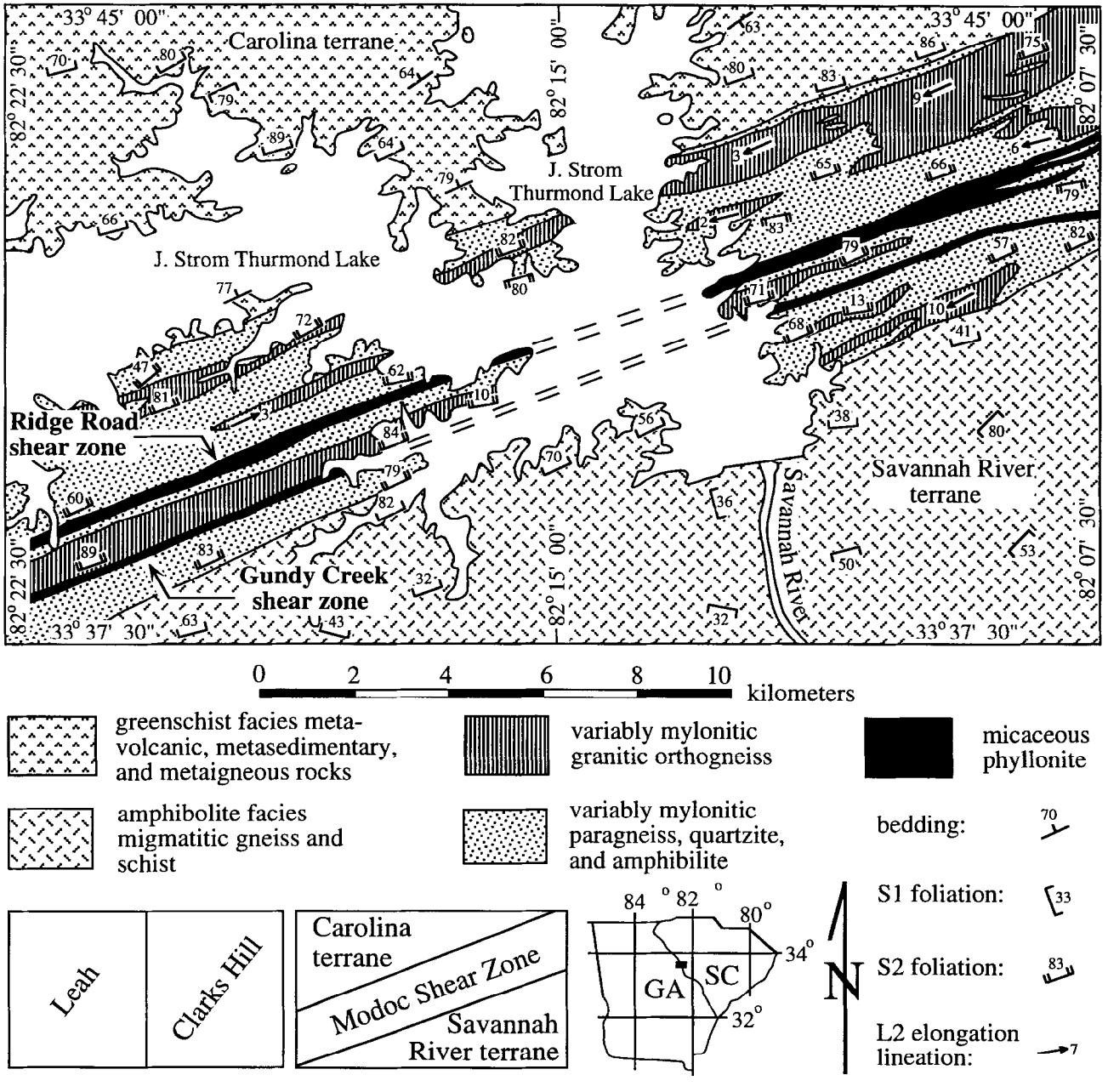

Fig. 6. Geological map of the Clarks Hill and Leah 7½′ quadrangles, South Carolina and Georgia, showing the locations of the Ridge Road and Gundy Creek shear zones, which are interpreted to be late Alleghanian (~275–290 Ma) in age and to overprint the early Alleghanian (~300–310 Ma) Modoc shear zone. Modified from Maher and Sacks (1987).

the late Paleozoic. In the J. Strom Thurmond Lake area, the Modoc shear zone is ~5 km thick and dips steeply northwest. U–Pb dating of synkinematic orthogneiss sheets (Pray, 1993), together with $^{40}Ar/^{39}Ar$ dating of recrystallized hornblende in mylonitic paragneisses (Dallmeyer *et al.*, 1986; Dallmeyer, personal communication 1989), indicate that the Modoc shear zone moved during ~290–310 Ma. Analysis of *S–L* fabrics in synkinematic orthogneiss sheets indicates a dominantly horizontal slip direction for the Modoc shear zone, and *S–C* relationships, asymmetric porphyroclasts and rotated tension gashes indicate a dextral sense of shear (Sacks and Dennis, 1987; Sacks, 1989).

The fabric elements associated with the Modoc shear zone (S_2, L_2, Fig. 6), as well as the synkinematic orthogneiss sheets in the Modoc shear zone, are locally folded by NW-vergent mesoscopic to macroscopic scale F_3 folds. These folds are interpreted (Maher, 1987) to be genetically related to northwestward translation above a regional décollement (Cook *et al.*, 1979; West *et al.*, 1995) that moved at ~300 Ma (Student and Sinha, 1992).

The Ridge Road and Gundy Creek shear zones are 100–500-m thick phyllonite zones contained within the southern part of the much thicker Modoc shear zone (Fig. 6). F_3 folds have not been observed to overprint the phyllonitic schistosity of the Ridge Road or Gundy Creek shear zones, and the shear zones are therefore interpreted to be D_4 structures. The phyllonites contain a penetrative schistosity (S_4) caused by parallel alignment of muscovite and biotite–chlorite. L_4 elongation lineations have not been observed in the Ridge Road or Gundy Creek shear zones. S_4 is cut by non-penetrative anastomosing C'_4 surfaces spaced 0.4–5.0 cm apart (Figs 7a & b and 8). The D_4 phyllonites are heterogeneous at micro- and mesoscales because of compositional layering parallel to S_4. In some layers muscovite (90–95%) predominates, whereas other layers are dominantly quartz (70%). Some of the quartz-rich layers may represent deformed and recrystallized veins or metamorphic segregations transposed into parallelism with S_4. Overall, muscovite and quartz predominate, with accessory biotite–chlorite, plagioclase, opaques, garnet, and trace schorlite, staurolite, cordierite (?) and perovskite (?) (Fig. 9). Away from C'_4 surfaces, quartz is polygonal and equant with weak undulose extinction. Along C'_4 surfaces, quartz is finer grained, has moderate undulose extinction and has grain shape anisotropy with aspect ratios up to 4:1 (Fig. 8a). Micas within C'_4 surfaces are shredded and are finer grained than they are away from C'_4. Garnet is locally retrogressed to chlorite (Fig. 8b), although chlorite appears to be in textural equilibrium with biotite. The above petrographic data are interpreted to indicate that the last stages of deformation in the D_4 shear zone took place during cooling through lower amphibolite and/or greenschist facies conditions, above the ~300°C brittle–ductile transition temperature for quartz (Simpson and De Paor, 1991), and under conditions where recovery processes were dominant over deformation processes outside C'_4 surfaces, but where deformation slightly predominated over recovery within C'_4 surfaces.

Maher *et al.* (1994) presented $^{40}Ar/^{39}Ar$ age spectra for whole-rock phyllonite from the Ridge Road shear zone and for muscovite from the Gundy Creek shear zone (Fig. 9). The sample from the Ridge Road shear zone displayed a 274.4 ± 1.0 Ma age plateau, which corresponded to 70% of the evolved argon, and which was interpreted to indicate the time of cooling through the ~400°C blocking temperature for argon retention in white mica making up 25% of the sample. The muscovite sample from the Gundy Creek shear zone displayed a 277.7 ± 0.4 Ma age plateau, which corresponded to 94% of the evolved argon, and which was interpreted to indicate the time of cooling through the ~400°C muscovite blocking temperature. The undisturbed $^{40}Ar/^{39}Ar$ age plateau manifested in the Gundy creek shear zone, together with the apparent absence of extraneous argon, are interpreted to indicate that the final stages of deformation in the Gundy creek shear zone took place above the muscovite blocking temperature. Maher *et al.* (1994) also reported four $^{40}Ar/^{39}Ar$ muscovite plateau ages from elsewhere in the Modoc shear zone and from the Savannah River terrane that were narrowly constrained to 272–278 Ma. Taken together, the fabric relationships, petrographic data and geochronological data described above are interpreted to indicate that the Ridge Road and Gundy Creek shear zones are substantially younger than the Modoc shear zone. The above $^{40}Ar/^{39}Ar$ muscovite cooling ages are interpreted to indicate that the rocks from the northern edge of the Modoc shear zone to the southern edge of the Savannah River terrane have been an intact structural unit since cooling through the muscovite blocking temperature at ~275 Ma, and that the last stages of deformation in the Ridge Road and Gundy Creek shear zones occurred immediately prior to ~275 Ma.

Data on the orientation of S_4 and C'_4 in the Ridge Road and Gundy Creek shear zones are given in Fig. 10. The orientation of the shear-zone boundaries are interpreted to be essentially vertical, and the displacement directions to be essentially horizontal because the average S_4 and C'_4 orientations are vertical. The average strikes of S_4 and C'_4 are, respectively, counterclockwise and clockwise from the inferred shear-zone boundaries. The dextral drag of S_4 foliae adjacent to C'_4 surfaces (Figs 7a & b and 8a) clearly indicates a dextral sense of shear for the zones as a whole.

The scatter evident in the orientations of C'_4 and S_4 are interpreted to indicate that the overall deformation in the Ridge Road and Gundy Creek shear zones was heterogeneous, and/or that steady-state deformation conditions were not attained throughout the Ridge Road or Gundy Creek shear zones. Nevertheless, the strong preferred orientations of C'_4 and S_4, respectively, clockwise and counterclockwise from the inferred shear-zone boundaries, are interpreted to indicate an inclined flow apophysis.

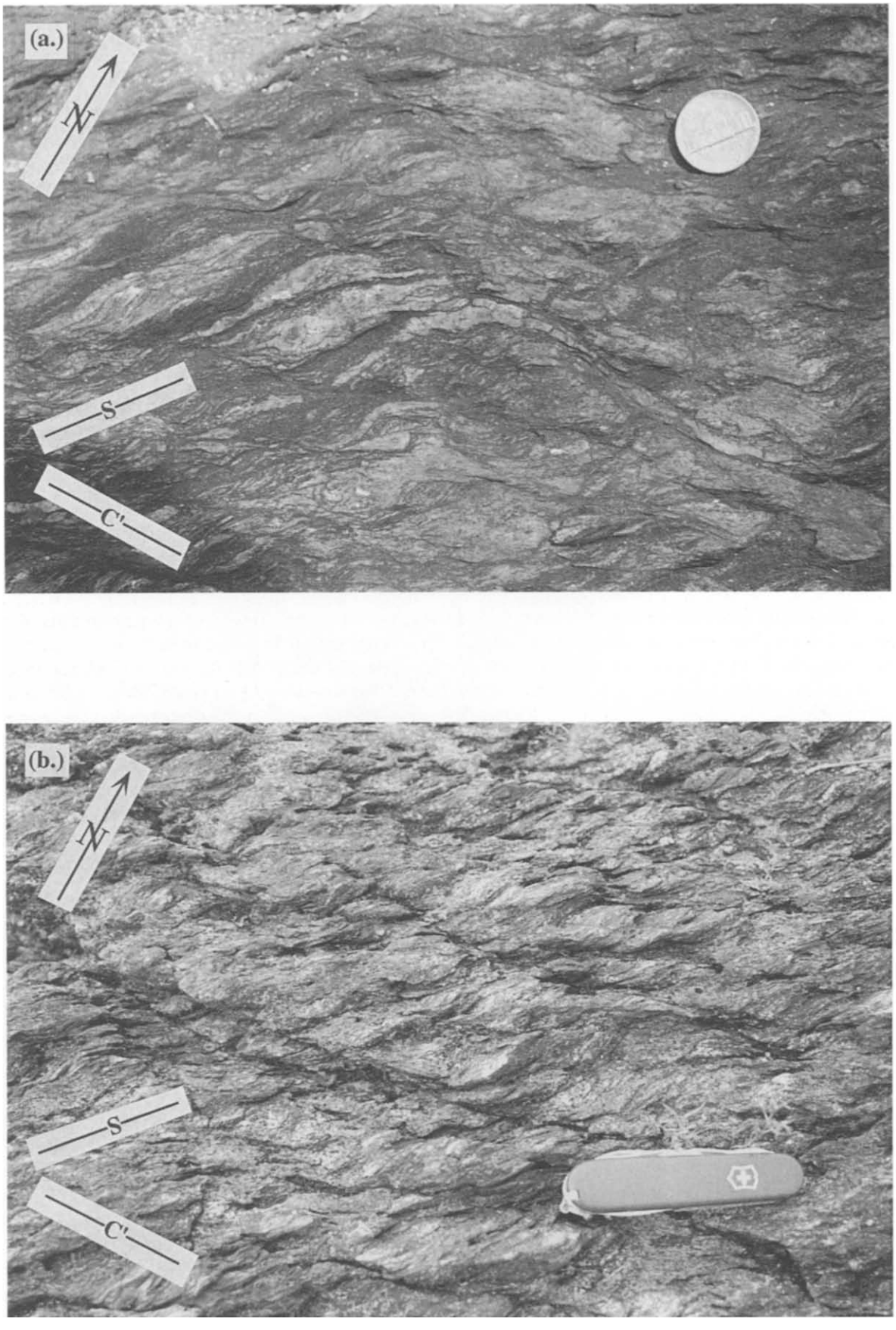

Fig. 7. Photographs of S–C_4' fabric relationships in the Ridge Road shear zone. (a) Clark Hill Quadrangle east of Clark Hill Lake. (b) Leah Quadrangle west of Clark Hill Lake.

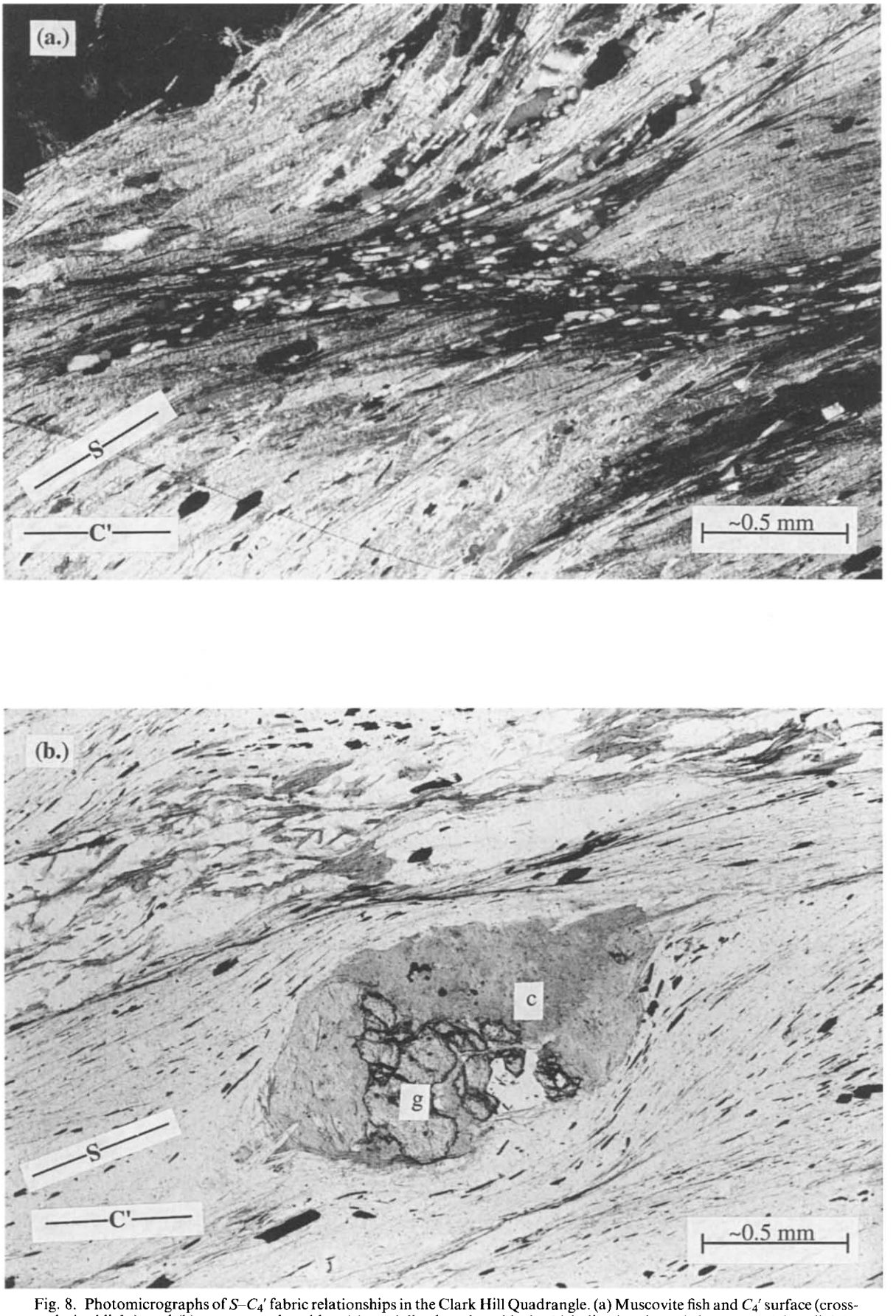

Fig. 8. Photomicrographs of S–C_4' fabric relationships in the Clark Hill Quadrangle. (a) Muscovite fish and C_4' surface (cross-polarized light); and (b) garnet porphyroblast (g) partially altered to chlorite (c) indicating dextral shear sense (plane light).

	GUNDY CREEK SHEAR ZONE	RIDGE ROAD SHEAR ZONE
mineral assemblage, in order of abundance	quartz, muscovite, biotite, opaques, schorlite, garnet, staurolite, chlorite	quartz, muscovite, plagioclase, garnet, biotite, penninite, opaques, perovskite(?)
$^{40}Ar/^{39}Ar$ muscovite plateau age, (Maher and others, 1994)	277.7 ± 0.4 Ma	274.4 ± 1.0 Ma
average S_4 attitude	N41°E 90°	N29°E 82°SE
average C'_4 attitude	N83°E 90°	N80°E 90°
attitude of shear zone boundaries	N70°E 90°	N70°E 88°SE

Fig. 9. Summary of selected petrographic, geochronological and structural data from the Gundy Creek and Ridge Road shear zones.

Evidence for synkinematic brittle faulting has not been found within or adjacent to the Ridge Road or Gundy Creek shear zones. Therefore, it is assumed that material compatibility was maintained during deformation. The field and geochronological data discussed in earlier paragraphs are interpreted to indicate that ductile deformation in the Modoc shear zone and in the Carolina and Savannah River terranes had ceased prior to the development of the Ridge Road and Gundy Creek shear zones. Therefore, it is reasonable to assume that stretching parallel to the shear zone walls did not take place during development of the Ridge Road and Gundy Creek shear zones. The regional consistency of D_2 fabric elements in the Modoc shear zone outside of the Ridge Road and Gundy Creek shear zones (Sacks and Dennis, 1987) indicates that there was no relative rotation of the shear-zone walls. The only deformational style that is consistent with the above boundary conditions is plane-strain convergent shear. Under these circumstances, eqn. (24) predicts that C' will be parallel to relative velocity vector of the walls bounding the Ridge Road and Gundy Creek shear zones. A vector oriented at ~10–13° clockwise from the shear zone walls is indicated (Fig. 10). Equation (21) can be used to predict the progressive rotation of C' surfaces during shear zone development. The example illustrated in Fig. 3 is chosen to simulate the Gundy Creek shear zone in which the stable C' orientation is 13° clockwise from the shear-zone boundary. Equations (22) and (A29) can be used to predict the progressive rotations of material planes and the flattening plane of the strain ellipsoid, respectively, during shear-zone development. The example illustrated in Fig. 4 is chosen to simulate the Gundy creek shear zone in which stable S is oriented approximately 29° counter-clockwise from the shear-zone boundary. Note that the predicted orientations for pre-existing material planes and for the flattening plane of the strain ellipsoid progressively converge as deformation increases.

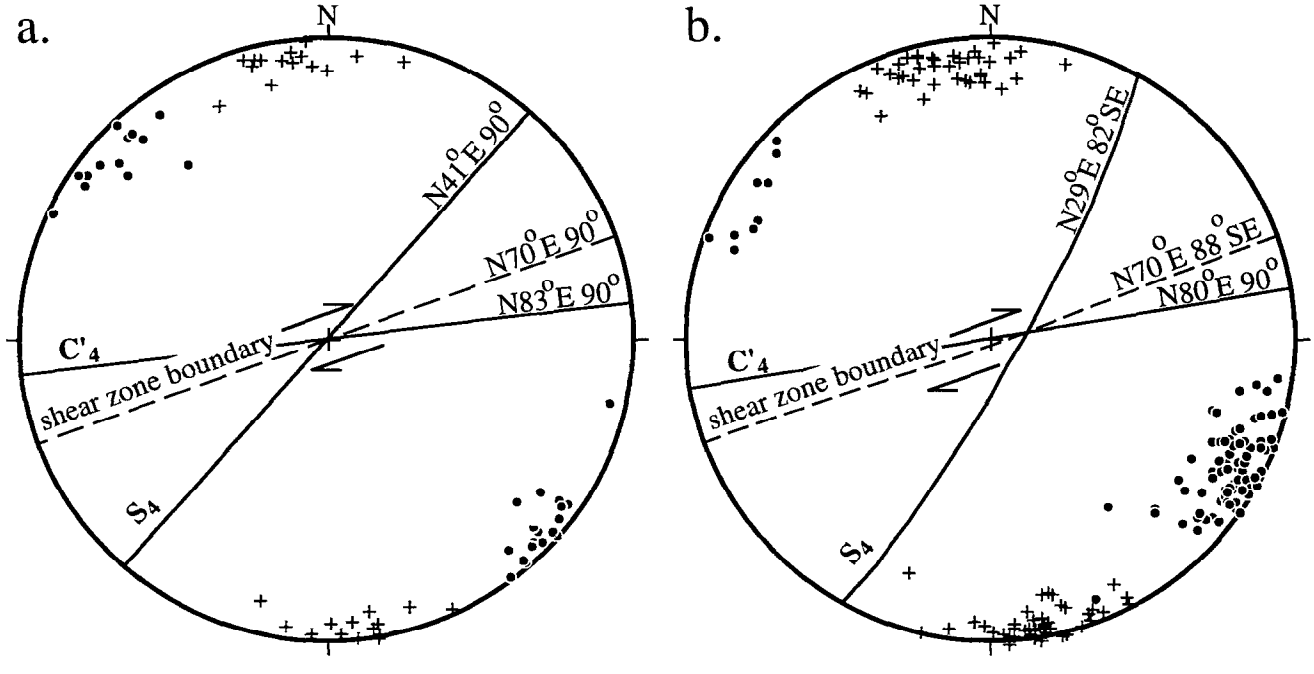

Fig. 10. Lower-hemisphere equal-area projections of structural data from the J. Strom Thurmond Lake area on the Savannah River, South Carolina and Georgia. (a) Scatter plot of poles to 31 S_4 planes (dots) and 31 C'_4 planes (crosses) from the Gundy Creek shear zone. (b) Scatter plot of poles to 91 S_4 planes (dots) and 91 C'_4 planes (crosses) from the Ridge Road shear zone. Planes parallel to the mean orientations of S_4 and C'_4 are shown. The orientations of the shear-zone boundary planes (dashed lines) are assumed parallel to both the map strike of the shear zones and to the corresponding lines of intersection of the mean S_4 and C'_4 planes.

CONCLUSIONS

(1) If a shear zone develops between rigid blocks which do not rotate relative to each other, and if compatibility is maintained within the zone and at its walls, then a steady-state fabric in which C' is inclined in the shear direction and S is oppositely inclined is indicative of convergent shear.

(2) Under the circumstances assumed above, but prior to the development of steady-state fabric, a preferred orientation of S and C' oppositely inclined to the shear-zone boundary may be indicative of convergent shear with the relative velocity vector of the opposing walls of the shear zone approximately parallel to the strongest preferred orientation of C'.

(3) Fabrics in the Ridge Road and Gundy Creek shear zones in the southern Appalachian Piedmont are suggestive of dextral convergent shear with a relative velocity vector of the opposing walls of the shear zone oriented ~ 10–13° clockwise from the strike of the shear zone.

Acknowledgements—This work is supported by National Science Foundation grants EAR 8803833 and EAR 9117468 to D. T. Secor, and EAR 8803675 and EAR 9117959 to H. D. Maher. We thank A. J. Dennis for providing support for Pray through SCUREF Task 170. We thank C. L. Secor for providing field photographs of S–C' relationships; R. W. Allmendinger for providing a copy of the academic version of his stereonet plotting program, version 4.5.2; T. G. Blenkinsop, A. J. Dennis, C. W. Passchier, B. Tikoff and T. E. West, Jr for helpful reviews and/or discussions.

REFERENCES

Berthé, D., Choukroune, P. and Jegouzo, P. (1979) Orthogneiss, mylonite and non coaxial deformation of granites: the example of the South Armorican shear zone. *Journal of Structural Geology* **1**, 31–42.

Berthé, D., Choukroune, P. and Gapais, D. (1979) Orientations préférentielles du quartz et orthogneissification progressive en régime cisaillant: l'example du cisaillement sud-armoricain. *Bulletin de Minéralogie* **102**, 265–272.

Blenkinsop, T. G. and Treloar, P. J. (1995) Geometry, classification and kinematics of S–C and S–C' fabrics in the Mushandike area, Zimbabwe. *Journal of Structural Geology* **17**, 397–408.

Bobyarchick, A. R. (1986) The eigenvalues of steady flow in Mohr space. *Tectonophysics* **122**, 35–51.

Cook, F. A., Albaugh, D. S., Brown, L. D., Kaufman, S., Oliver, J. E. and Hatcher, R. D. (1979) Thin-skinned tectonics in the crystalline southern Appalachians; COCORP seismic-reflection profiling of the Blue Ridge and Piedmont. *Geology* **7**, 563–567.

Dallmeyer, R. D., Wright, J. E., Secor, D. T. and Snoke, A. W. (1986) Character of the Alleghanian orogeny in the southern Appalachians: Part II. Geochronological constraints on the tectonothermal evolution of the eastern Piedmont in South Carolina. *Bulletin of the Geological Society of America* **97**, 1329–1344.

Davison, I., McCarthy, M., Powell, D., Torres, H. H. F. and Santos, C. A. (1995) Laminar flow in shear zones: the Pernambuco shear zone, NE-Brazil. *Journal of Structural Geology* **17**, 149–161.

Dennis, A. J., Sacks, P. E. and Maher, H. D. (1987) Nature of the late Alleghanian strike-slip deformation in the eastern South Carolina Piedmont: The Irmo shear zone. In *Anatomy of the Alleghanian Orogeny as Seen From the Piedmont of South Carolina and Georgia*, ed. D. T. Secor, Jr, pp. 49–66. Carolina Geological Society Field Trip Guidebook for 1987. South Carolina Geological Survey, Columbia.

Dennis, A. J. and Secor, D. T. (1987) A model for the development of crenulations in shear zones with applications from the southern Appalachian Piedmont. *Journal of Structural Geology* **9**, 809–817.

Dennis, A. J. and Secor, D. T. (1990) On resolving shear direction in foliated rocks deformed by simple shear. *Bulletin of the Geological Society of America* **102**, 1257–1267.

Flinn, D. (1978) Construction and computation of three-dimensional progressive deformations. *Journal of the Geological Society of London* **135**, 291–305.

Fossen, H. and Tikoff, B. (1993) The deformation matrix for simultaneous simple shearing, pure shearing and volume change, and its application to transpression–transtension tectonics. *Journal of Structural Geology* **15**, 413–422.

Lacassin, R. (1987) Kinematics of ductile shearing from outcrop to crustal scale in the Monte Rosa Nappe, western Alps. *Tectonics* **6**, 69–88.

Leon, S. J. (1990) *Linear Algebra With Applications*. Macmillan, New York.

Lister, G. S. and Snoke, A. W. (1984) S-C mylonites. *Journal of Structural Geology* **6**, 617–638.

Maher, H. D. (1987) D_3 folding in the eastern Piedmont associated with Alleghanian thrusting. In *Anatomy of the Alleghanian Orogeny as Seen From the Piedmont of South Carolina and Georgia*, ed. D. T. Secor, Jr, pp. 35–48. Carolina Geological Society Field Trip Guidebook for 1987. South Carolina Geological Survey, Columbia.

Maher, H. D., Dallmeyer, R. D., Secor, D. T. and Sacks, P. E. (1994) $^{40}Ar/^{39}Ar$ constraints on chronology of Augusta fault zone movement and late Alleghanian extension, southern Appalachian Piedmont, South Carolina and Georgia. *American Journal of Science* **294**, 428–448.

Maher, H. and Sacks, P. (1987) Geologic map of the Clarks Hill and Leah Quadrangles, SC and GA. In *Anatomy of the Alleghanian Orogeny as Seen From the Piedmont of South Carolina and Georgia*, ed. D. T. Secor, Jr, Plate 1, scale 1:40 000. Carolina Geological Society Field Trip Guidebook for 1987. South Carolina Geological Survey, Columbia.

O'Hara, K. (1988) Fluid flow and volume loss during mylonitization: an origin for phyllonite in an overthrust setting, North Carolina, U.S.A. *Tectonophysics* **156**, 21–36.

O'Hara, K. (1990) State of strain in mylonites from the western Blue Ridge province, southern Appalachians: the role of volume loss. *Journal of Structural Geology* **12**, 419–430.

Passchier, C. W. (1991) Geometric constraints on the development of shear bands in rocks. *Geologie Mijnbouw* **70**, 203–211.

Passchier, C. W. and Urai, J. L. (1988) Vorticity and strain analysis using Mohr diagrams. *Journal of Structural Geology* **10**, 755–763.

Platt, J. P. and Vissers, R. L. M. (1980) Extensional structures in anisotropic rocks. *Journal of Structural Geology* **2**, 397–410.

Pray, J. R. (1993) U–Pb geochronology of the Modoc shear zone and adjacent terranes in the southeastern Appalachian Piedmont. Unpublished M.Sc. thesis, University of South Carolina, Columbia.

Ramsay, J. G. (1980) Shear zone geometry: a review. *Journal of Structural Geology* **2**, 83–99.

Ramsay, J. G. and Allison, I. (1979) Structural analysis of shear zones in an alpinised Hercynian granite (Maggia Lappen, Penninc zone, central Alps). *Schweizerische mineralogische und petrographische Mitteilurgen* **59**, 251–279.

Ramsay, J. G. and Graham, R. H. (1970) Strain variation in shear belts. *Canadian Journal of Earth Sciences* **7**, 786–813.

Sacks, P. E. (1989) Geology of the eastern Piedmont along the Savannah River and implications for Appalachian tectonics. Unpublished Ph.D. thesis, University of South Carolina, Columbia, South Carolina.

Sacks, P. E. and Dennis, A. J. (1987) The Modoc zone—D_2 (early Alleghanian) in the eastern Appalachian Piedmont, South Carolina and Georgia. In *Anatomy of the Alleghanian Orogeny as Seen From the Piedmont of South Carolina and Georgia*, ed. D. T. Secor, Jr, pp. 19–34. Carolina Geological Society Field Trip Guidebook for 1987. South Carolina Geological Survey, Columbia.

Secor, D. T., Jr and Snoke, A. W. (1978) Stratigraphy, structure, and plutonism in the central South Carolina Piedmont. In *Geological Investigations of the Eastern Piedmont, Southern Appalachians*, ed. A. W. Snoke, pp. 65–123. Carolina Geological Society Field Trip Guidebook for 1978. South Carolina Geological Survey, Columbia.

Secor, D. T., Snoke, A. W., Bramlett, K. W., Costello, O. P. and Kimbrell, O. P. (1986) Character of the Alleghanian orogeny in the southern Appalachians: Part I. Alleghanian deformation in the eastern Piedmont of South Carolina. *Bulletin of the Geological Society of America* **97**, 1319–1328.

Simpson, C. and Schmid, S. M. (1983) An evaluation of criteria to deduce the sense of movement in sheared rocks. *Bulletin of the Geological Society of America* **94**, 1281–1288.

Simpson, C. and De Paor, D. (1991) *Deformation and kinematics of high strain zones*, pp. 1–116. Geological Society of America Short Course Notes.

Simpson, C. and De Paor, D. G. (1993) Strain and kinematic analysis in general shear zones. *Journal of Structural Geology* **15**, 1–20.

Student, J. J. and Sinha, A. K. (1992) Carboniferous U–Pb ages of zircons from the Box Ankle and Ocmulgee faults, central Georgia: Implications for accretionary models. *Geological Society of America Abstracts with Programs* **24**, 69.

Wallis, S. R. (1992) Vorticity analysis in a metachert from the Sanbagawa Belt, SW Japan. *Journal of Structural Geology* **14**, 271–280.

West, T. E., Secor, D. T., Pray, J. R., Boland, I. B. and Maher, H. D. (1995) New field evidence for an exposure of the Appalachian decollement at the east end of the Pine Mountain terrane, Georgia. *Geology* **23**, 621–624.

White, S. H., Burrows, S. E., Carreras, J., Shaw, N. D. and Humphreys, F. J. (1980) On mylonites in ductile shear zones. *Journal of Structural Geology* **2**, 175–187.

APPENDIX A

Digression on the calculation of eigenvalues and eigenvectors in R^2

Finite displacement field equations (derived from constant velocity field equations), and principal axes of strain can be determined by eigenanalysis. Here we derive generalized eigenvalues and the respective eigenvectors for a 2×2 real matrix.

Given the equation:

$$\mathbf{x}' = \mathbf{M}\mathbf{x} = \begin{bmatrix} x_1' \\ x_2' \end{bmatrix} = \begin{bmatrix} m_{11} & m_{12} \\ m_{21} & m_{22} \end{bmatrix} \begin{bmatrix} x_1 \\ x_2 \end{bmatrix}, \tag{A1}$$

the *eigenvalues* (λs) and *eigenvectors* (**v**s) are solutions of the equation

$$\mathbf{M}\mathbf{v} = \lambda\mathbf{v} = \lambda \begin{bmatrix} v_1 \\ v_2 \end{bmatrix}, \tag{A2}$$

where $\mathbf{v} \neq \mathbf{0}$. In other words, we are looking for vectors in which the transformation matrix contracts to a scalar value. Rewriting eqn. (A2) as:

$$\mathbf{M}\mathbf{v} - \lambda\mathbf{v} = (\mathbf{M} - \lambda\mathbf{I})\mathbf{v} = \mathbf{0} = \begin{bmatrix} m_{11} - \lambda & m_{12} \\ m_{21} & m_{22} - \lambda \end{bmatrix} \begin{bmatrix} v_1 \\ v_2 \end{bmatrix} = \begin{bmatrix} 0 \\ 0 \end{bmatrix}, \tag{A3}$$

we may observe that because $\mathbf{v} \neq \mathbf{0}$, then

$$|\mathbf{M} - \lambda\mathbf{I}| = 0. \tag{A4}$$

Expansion of the above equation yields the *characteristic equation*:

$$\lambda^2 - \lambda(m_{11} + m_{22}) + m_{11}m_{22} - m_{12}m_{21} = 0. \tag{A5}$$

Solving the quadratic equation for the eigenvalues yields:

$$\lambda_1 = \frac{m_{11} + m_{22} + \sqrt{(m_{11} - m_{22})^2 + 4m_{12}m_{21}}}{2}$$
$$\lambda_2 = \frac{m_{11} + m_{22} - \sqrt{(m_{11} - m_{22})^2 + 4m_{12}m_{21}}}{2}. \tag{A6}$$

It may be noted that the eigenvalues of a diagonal or triangular matrix are the elements of the principal diagonal. To determine the eigenvectors, we expand eqn. (A3) yielding two constraining equations:

$$(m_{11} - \lambda)v_1 + m_{12}v_2 = 0$$
$$m_{21}v_1 + (m_{22} - \lambda)v_2 = 0. \tag{A7}$$

Because of eqn. (A4) the two equations are singular and in many cases either may be used in determining the eigenvectors: the choice being made so as not to yield a trivial solution. In non-degenerate cases, there will be two sets of eigenvectors (for a 2×2 matrix) which are not collinear. An example of a degenerate case, where there is only one set of collinear eigenvectors, would be when all displacement in the reference plane occurs parallel to a line. Solving for v_2 as a function of v_1, where $v_1 = \kappa \neq 0$ is an arbitrary constant, and writing the above equations in vector form yields:

$$\mathbf{v} = \kappa \begin{bmatrix} 1 \\ \dfrac{\gamma - m_{11}}{m_{12}} \end{bmatrix} \quad \text{or} \quad \mathbf{v} = \kappa \begin{bmatrix} 1 \\ \dfrac{m_{21}}{\lambda - m_{22}} \end{bmatrix}. \tag{A8}$$

Therefore, for each eigenvalue, there is an associated set of eigenvectors; each eigenvector in the set is parallel to the other eigenvectors of the set. This can be verified by noting that (Leon, 1990):

$$\mathbf{M}(\kappa\mathbf{v}) = \kappa\mathbf{M}\mathbf{v} = \kappa\lambda\mathbf{v} = \lambda(\kappa\mathbf{v}). \tag{A9}$$

Letting $\kappa = 1$ we may easily write expressions for the counterclockwise angle, θ, an eigenvector makes with the positive x_1 axis (assuming a right-handed co-ordinate system):

$$\theta = \tan^{-1}\left(\frac{\lambda - m_{11}}{m_{12}}\right) \quad \text{or} \quad \theta = \tan^{-1}\left(\frac{m_{21}}{\lambda - m_{22}}\right). \tag{A10}$$

Also potentially useful is to let κ assume the reciprocal value of the length of **v** (i.e. $\kappa = \|\mathbf{v}\|^{-1}$), thus obtaining the unit eigenvectors ($\hat{\mathbf{v}}$'s):

$$\hat{\mathbf{v}} = \frac{1}{\sqrt{\left(\dfrac{\lambda - m_{11}}{m_{12}}\right)^2 + 1}} \begin{bmatrix} 1 \\ \dfrac{\lambda - m_{11}}{m_{12}} \end{bmatrix} \text{ or } \hat{\mathbf{v}} = \frac{1}{\sqrt{\left(\dfrac{m_{21}}{\lambda - m_{22}}\right)^2 + 1}} \begin{bmatrix} 1 \\ \dfrac{m_{21}}{\lambda - m_{22}} \end{bmatrix}. \tag{A11}$$

Calculation of finite displacement field equation

The velocity field equation for deformation within a plane can be written:

$$\dot{\mathbf{x}} = \dot{\mathbf{D}}\mathbf{x} \tag{A12a}$$

or in expanded form

$$\begin{bmatrix} \dfrac{\partial x_1}{\partial t} \\ \dfrac{\partial x_2}{\partial t} \end{bmatrix} = \begin{bmatrix} \dfrac{\partial \epsilon_{11}}{\partial t} & \dfrac{\partial \gamma_{12}}{\partial t} \\ \dfrac{\partial \gamma_{21}}{\partial t} & \dfrac{\partial \epsilon_{22}}{\partial t} \end{bmatrix} \begin{bmatrix} x_1 \\ x_2 \end{bmatrix} = \begin{bmatrix} \dot{\epsilon}_{11} & \dot{\gamma}_{12} \\ \dot{\gamma}_{21} & \dot{\epsilon}_{22} \end{bmatrix} \begin{bmatrix} x_1 \\ x_2 \end{bmatrix}, \tag{A12b}$$

where the column vectors composing $\dot{\mathbf{D}}$ are the rates of displacement of elemental vectors initially parallel to the co-ordinate axes. The solution of the differential eqn. (A12) yields a finite displacement field equation for position (**x**) as a function of a parameter t, herein conveniently considered as time:

$$\mathbf{x}(t) = \mathbf{D}(t)\mathbf{x}(0) \tag{A13a}$$

or in expanded form

$$\begin{bmatrix} x_1(t) \\ x_2(t) \end{bmatrix} = \begin{bmatrix} 1 + \epsilon_{11} & \gamma_{12} \\ \gamma_{21} & 1 + \epsilon_{22} \end{bmatrix} \begin{bmatrix} x_1(0) \\ x_2(0) \end{bmatrix}. \tag{A13b}$$

Note that the elements on the principal diagonal of **D** are the stretches parallel to the respective co-ordinate axes, and the elements on the left diagonal are shear strains.

If we assume that the velocity components of eqn. (A12) are constants, eqn. (A13) may be determined using eigenanalysis. From eqn. (A6) the eigenvalues of $\dot{\mathbf{D}}$ are:

$$\lambda_1 = \frac{\dot{\epsilon}_{11} + \dot{\epsilon}_{22} + \sqrt{(\dot{\epsilon}_{11} - \dot{\epsilon}_{22})^2 + 4\dot{\gamma}_{12}\dot{\gamma}_{21}}}{2}$$
$$\lambda_2 = \frac{\dot{\epsilon}_{11} + \dot{\epsilon}_{22} - \sqrt{(\dot{\epsilon}_{11} - \dot{\epsilon}_{22})^2 + 4\dot{\gamma}_{12}\dot{\gamma}_{21}}}{2} \tag{A14}$$

From eqn. (A8) the eigenvectors of $\dot{\mathbf{D}}$ are (letting $\kappa = 1$):

$$\mathbf{v} = \begin{bmatrix} 1 \\ \dfrac{\lambda - \dot{\epsilon}_{11}}{\dot{\gamma}_{12}} \end{bmatrix} \quad \text{or} \quad \mathbf{v} = \begin{bmatrix} 1 \\ \dfrac{\dot{\gamma}_{21}}{\lambda - \dot{\epsilon}_{22}} \end{bmatrix}. \tag{A15}$$

The general solution of eqn. (A12) will be of the form (cf. Leon, 1990):

$$\mathbf{x}(t) = c_1\mathbf{v}_{(1)}e^{\lambda_1 t} + c_2\mathbf{v}_{(2)}e^{\lambda_2 t} \tag{A16a}$$

or in expanded form

$$\begin{bmatrix} x_1(t) \\ x_2(t) \end{bmatrix} = \begin{bmatrix} c_1 v_{(1)1}e^{\lambda_1 t} + c_2 v_{(2)1}e^{\lambda_2 t} \\ c_1 v_{(1)2}e^{\lambda_1 t} + c_2 v_{(2)2}e^{\lambda_2 t} \end{bmatrix}, \tag{A16b}$$

where $\mathbf{v}_{(1)}$, $\mathbf{v}_{(2)}$ are the eigenvectors of $\dot{\mathbf{D}}$ corresponding to the eigenvalues λ_1, λ_2, and c_1 and c_2 are arbitrary constants. An exact solution may be determined by substitution of the initial conditions $\{x(t) = x(0)|t = 0\}$ into eqn. (A16) and solving for c_1 and c_2

$$\begin{bmatrix} x_1(0) \\ x_2(0) \end{bmatrix} = \begin{bmatrix} c_1 v_{(1)1} + c_2 v_{(2)1} \\ c_1 v_{(1)2} + c_2 v_{(2)2} \end{bmatrix}, \tag{A17}$$

therefore

$$\begin{aligned} c_1 &= \frac{1}{|\mathbf{V}|}\left[v_{(2)2}x_1(0) - v_{(2)1}x_2(0)\right] \\ c_2 &= \frac{1}{|\mathbf{V}|}\left[v_{(1)1}x_2(0) - v_{(1)2}x_1(0)\right], \end{aligned} \tag{A18}$$

where

$$|\mathbf{V}| = \left[v_{(1)1}v_{(2)2} - v_{(1)2}v_{(2)1}\right]. \tag{A19}$$

Back substitution of c_1 and c_2 into eqn. (A16) and writing in matrix form yields:

$$\begin{bmatrix} x_1(t) \\ x_2(t) \end{bmatrix} = \frac{1}{|\mathbf{V}|}\begin{bmatrix} v_{(1)1}v_{(2)2}e^{\lambda_1 t} - v_{(1)2}v_{(2)1}e^{\lambda_2 t} & v_{(1)1}v_{(2)1}\left(e^{\lambda_2 t} - e^{\lambda_1 t}\right) \\ v_{(2)2}v_{(1)2}\left(e^{\lambda_1 t} - e^{\lambda_2 t}\right) & v_{(1)1}v_{(2)2}e^{\lambda_2 t} - v_{(1)2}v_{(2)1}e^{\lambda_1 t} \end{bmatrix} \times \begin{bmatrix} x_1(0) \\ x_2(0) \end{bmatrix}. \tag{A20}$$

Equation (A20) maps the displacement of a point or position vector, $\mathbf{x}(t)$, at any time we wish to consider. If we allow the elements $[\mathbf{x}(t)]^{\mathrm{T}}$ to contain the co-ordinates of a normal vector to a plane, we may write an expression describing the displacement of the normal to the plane as a function of time by noting that (Flinn, 1978):

$$\begin{bmatrix} x_1(t) \\ x_2(t) \end{bmatrix}^{\mathrm{T}} = \begin{bmatrix} x_1(0) \\ x_2(0) \end{bmatrix}^{\mathrm{T}} \begin{bmatrix} 1+\epsilon_{11} & \gamma_{12} \\ \gamma_{21} & 1+\epsilon_{22} \end{bmatrix}^{-1} \tag{A21}$$

or

$$\begin{bmatrix} x_1(t) \\ x_2(t) \end{bmatrix}^{\mathrm{T}} = \begin{bmatrix} x_1(0) \\ x_2(0) \end{bmatrix}^{\mathrm{T}} \frac{|\mathbf{V}|}{|\mathbf{D}|} \times \begin{bmatrix} v_{(1)1}v_{(2)2}e^{\lambda_2 t} - v_{(1)2}v_{(2)1}e^{\lambda_1 t} & v_{(1)1}v_{(2)1}\left(e^{\lambda_1 t} - e^{\lambda_2 t}\right) \\ v_{(2)2}v_{(1)2}\left(e^{\lambda_2 t} - e^{\lambda_1 t}\right) & v_{(1)1}v_{(2)2}e^{\lambda_1 t} - v_{(1)2}v_{(2)1}e^{\lambda_2 t} \end{bmatrix}, \tag{A22}$$

where

$$|\mathbf{D}| = \begin{bmatrix} v_{(1)1}v_{(2)2}e^{\lambda_1 t} - v_{(1)2}v_{(2)1}e^{\lambda_2 t} & v_{(1)1}v_{(2)1}\left(e^{\lambda_2 t} - e^{\lambda_1 t}\right) \\ v_{(2)2}v_{(1)2}\left(e^{\lambda_1 t} - e^{\lambda_2 t}\right) & v_{(1)1}v_{(2)2}e^{\lambda_2 t} - v_{(1)2}v_{(2)1}e^{\lambda_1 t} \end{bmatrix}. \tag{A23}$$

The counterclockwise angle, θ_t, a position vector or normal vector to a plane makes with the positive x_1 axis at a point in time (t) is:

$$\theta_t = \tan^{-1}\frac{x_2(t)}{x_1(t)}. \tag{A24}$$

If we allow $\mathbf{x}(0)$ to have an initial length of unity, then:

$$x_1(0) = \cos\theta_0 \tag{A25}$$

and

$$x_2(0) = \sin\theta_0. \tag{A26}$$

Substitution of the initial conditions into eqn. (A20) and solving for $\tan\theta_t$ in eqn. (A24) yields the orientation position vector as a function of time:

$$\tan\theta_t = \frac{v_{(2)2}v_{(1)2}\left(e^{\lambda_1 t} - e^{\lambda_2 t}\right) + \left(v_{(1)1}v_{(2)2}e^{\lambda_2 t} - v_{(1)2}v_{(2)1}e^{\lambda_1 t}\right)\tan\theta_0}{v_{(1)1}v_{(2)2}e^{\lambda_1 t} - v_{(1)2}v_{(2)1}e^{\lambda_2 t} + \left(v_{(1)1}v_{(2)2}e^{\lambda_2 t} - v_{(1)2}v_{(2)1}e^{\lambda_1 t}\right)\tan\theta_0}. \tag{A27}$$

Similarly, using eqn. (A22) we may write an expression for the orientation of the normal to a plane as a function of time:

$$\tan\theta_t = \frac{v_{(1)1}v_{(2)1}\left(e^{\lambda_1 t} - e^{\lambda_2 t}\right) + \left(v_{(1)1}v_{(2)2}e^{\lambda_1 t} - v_{(1)2}v_{(2)1}e^{\lambda_2 t}\right)\tan\theta_0}{\left(v_{(1)1}v_{(2)2}e^{\lambda_2 t} - v_{(1)2}v_{(2)1}e^{\lambda_1 t}\right) + v_{(2)2}v_{(1)2}\left(e^{\lambda_2 t} - e^{\lambda_1 t}\right)\tan\theta_0}. \tag{A28}$$

Calculation of principal axes of the finite strain ellipse

The principal axes of the finite strain ellipse are determined by calculating the eigenvectors and corresponding eigenvalues of the composition of the finite displacement matrix and its transpose (Fossen and Tikoff, 1993), viz.:

$$\mathbf{D}\mathbf{D}^{\mathrm{T}} = \begin{bmatrix} (1+\epsilon_{11})^2 + \gamma_{12}^2 & (1+\epsilon_{11})\gamma_{21} + (1+\epsilon_{22})\gamma_{12} \\ (1+\epsilon_{11})\gamma_{21} + (1+\epsilon_{22})\gamma_{12} & (1+\epsilon_{22})^2 + \gamma_{21}^2 \end{bmatrix}. \tag{A29}$$

The eigenvalues of $\mathbf{D}\mathbf{D}^{\mathrm{T}}$ are the magnitudes of the principal quadratic elongations, which are directed parallel to the corresponding eigenvectors.